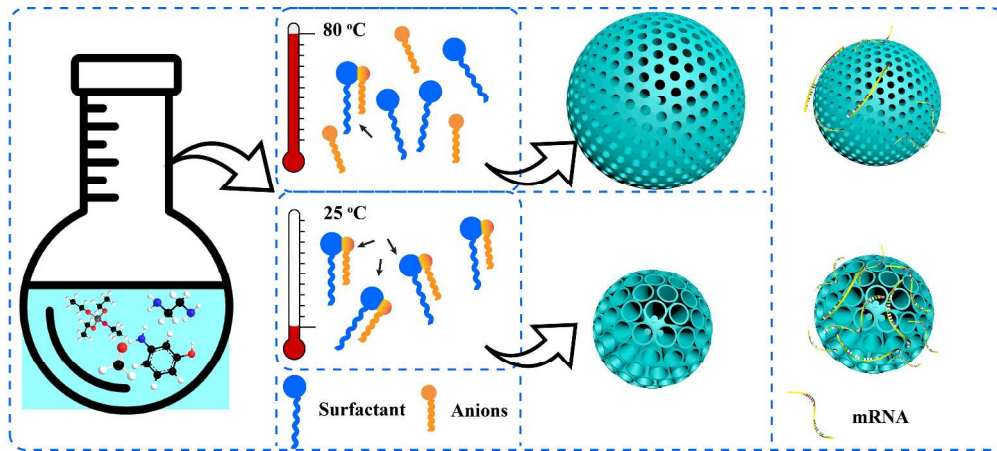




Room temperature synthesis of dendritic mesoporous silica nanoparticles with small sizes and enhanced mRNA delivery performance

Journal:	<i>Journal of Materials Chemistry B</i>
Manuscript ID	TB-ART-02-2018-000544.R1
Article Type:	Paper
Date Submitted by the Author:	03-May-2018
Complete List of Authors:	<p>Wang, Yue; University of Queensland, Australian Institute for Bioengineering and Nanotechnology (AIBN)</p> <p>Song, Hao; The University of Queensland, Australian Institute for Bioengineering and Nanotechnology</p> <p>Yu, Meihua; The University of Queensland, Australian Institute for Bioengineering and Nanotechnology (AIBN)</p> <p>Xu, Chun; University of Queensland, Australian Institute for Bioengineering and Nanotechnology (AIBN),</p> <p>Liu, Yang; Australian Institute for Bioengineering and Nanotechnology (AIBN), University of Queensland</p> <p>Tang, Jie; The University of Queensland, AIBN</p> <p>Yang, Yannan; The University of Queensland, Australian Institute for Bioengineering and Nanotechnology (AIBN)</p> <p>Yu, Chengzhong; University of Queensland, Australian Institute for Bioengineering and Nanotechnology (AIBN)</p>



518x229mm (300 x 300 DPI)



Journal Name

ARTICLE

Room temperature synthesis of dendritic mesoporous silica nanoparticles with small sizes and enhanced mRNA delivery performance

Received 00th January 20xx,
Accepted 00th January 20xx

DOI: 10.1039/x0xx00000x

www.rsc.org/

Yue Wang,^a Hao Song,^a Meihua Yu,^a Chun Xu,^a Yang Liu,^a Jie Tang,^a Yinnan Yang,^a and Chengzhong Yu^{*a}

Dendritic mesoporous silica nanoparticles (DMSNs) with a small diameter (~50 nm) and large pore size (>20 nm) have been synthesized at room temperature. It is shown that the choice of room temperature synthesis favours the formation of the large-pore and small-size DMSNs than conventional synthesis at higher temperature. Compared to mesoporous silica nanoparticles with a similar particle size but smaller mesopore size and DMSNs with a similar pore size but larger particle size, the DMSNs with both a small particle size and large pore size possess a higher *in vitro* mRNA transfection efficiency, indicating their potential as promising delivery vehicles for exogenous genetic molecules.

Introduction

Mesoporous silica nanoparticles (MSNs) are recognized as promising delivery systems for biomedical applications owing to their controllable structures,¹ excellent biocompatibility² and easy surface functionalization with desired property.³ The structural parameters of MSNs play crucial roles in their cargo loading and cellular uptake performance, important for intracellular drug delivery. For example, MSNs with a diameter of 50 nm have been demonstrated with maximum cellular uptake efficiency.⁴⁻⁵ Furthermore, MSNs with a large pore size (>20 nm) exhibited enhanced loading and transfection towards plasmid DNA molecules compared to MSNs with a small mesopore of 2 nm.⁶ Despite substantial progresses have been made in the synthesis of MSNs with diameters of ca. 50 nm,^{5,7-8} their pore sizes are limited, which impairs their associated loading capability and delivery efficacy of macromolecules.^{6,9} Recently, a new class of MSNs with dendritic central-radial pore channels (DMSNs) has attracted increasing attention due to their unique open and accessible large pores.¹⁰ Significant advances have been made in the pore size¹¹⁻¹⁸ and morphology control over the DMSNs.^{14, 18} However, the synthesis of monodispersed DMSNs with particle sizes around 50 nm with large pores (>20 nm) is rarely reported. Moreover, almost all previous reports realised the synthesis of DMSNs at elevated

temperature in either biphasic or aqueous solution synthesis.^{1-13-14, 18} There is no report on the synthesis of DMSNs at room temperature.

Herein, we report that DMSNs with a small particle size of ~50 nm and large dendritic pores of ~20 nm on the surface can be synthesized at room temperature. Compared to previous reports on the synthesis of DMSNs at an elevated reaction temperature (e.g., 80 °C),^{13, 15-16, 19} it is demonstrated that the room temperature favours the formation of large-pore dendritic structures. Moreover, a lower temperature is essential for the formation of DMSNs with smaller sizes. Furthermore, it is demonstrated that the DMSNs with both a small particle size and large pore size possess an overall enhanced mRNA delivery efficacy than either MSNs with a similar particle size but smaller pore size or DMSNs with a similar pore size but large particle size.

Experimental

Materials and reagents

Cetyltrimethylammonium bromide (CTAB), triethanolamine (TEA), tetraethyl orthosilicate (TEOS, 98%), sodium 3-(trihydroxysilyl) propylmethylphosphonate (THPMP), polyethylenimine (PEI, branched, molecular weight: 10000) and phosphate buffer solution (PBS, 10 mM, pH 7.4) were purchased from Sigma-Aldrich. Sodium heptafluorobutyrate (FC4) was purchased from Santa Cruz Biotechnology. mRNA encoding enhanced green fluorescent protein (EGFP) (996 nucleotides) was purchased from Trilink Biotechnologies. The Vybrant Dil cell labelling solution was purchased from Thermofisher Scientific.

^aAustralian Institute for Bioengineering and Nanotechnology, The University of Queensland, Brisbane, QLD 4072, Australia. E-mail: c.yu@uq.edu.au; Fax: +61-7-334 63973; Tel: +61-7-334 63283

Electronic Supplementary Information (ESI) available: Supporting figures and tables. See DOI: 10.1039/x0xx00000x

Synthesis of MSNs

In a typical synthesis, 380 mg of CTAB and a certain amount of FC4 were added into 25 mL of deionized water containing 68 mg of TEA and stirred at room temperature (RT) or 80 °C. After addition of 4 mL of TEOS, the solution was further stirred for 24 h at RT or 2 h at 80 °C. Products were collected after centrifugation, followed by calcination at 550 °C for 6 h in air to remove the surfactant. The final products are denoted MSNs-RT-*R* and MSNs-80-*R*, where RT and 80 refer to the synthesis temperature, *R* represents the molar ratio of FC4 to CTAB.

PEI modification of MSNs

For PEI modification, 30 mg of MSNs were dispersed into 10 mL of water (pH=10 adjusted with ammonium hydroxide), then 10 mL of 56 mM THPMP solution was added into the particle solution and stirring at 40 °C for 2 h to achieve surface modification of phosphonate groups. After centrifugation and thorough washing, the product was re-suspended in 15 mL of carbonate buffer solution (100 mM, pH=9.6) containing 150 mg of PEI (10 k). After stirring for 4 h at room temperature, the PEI modified MSNs were obtained by centrifugation, water washing and drying overnight at room temperature.

Characterization

Transmission electron microscopy (TEM) images were taken using JEOL 1010 operated at 100 kV. Before measurement, samples were dispersed in ethanol and then dried on carbon film supported copper grid. Scanning electron microscope (SEM) measurements were conducted using JEOL JSM 7800 field-emission scanning electron microscope (FE-SEM). For preparation, samples were dispersed in ethanol, then dropped to aluminium foil pieces which were attached to conductive carbon film on SEM mount. The SEM mount was dried in the vacuum oven at 60 °C for at least 12 h before characterization. Nitrogen adsorption-desorption measurement was conducted by a Micromeritics Tristar II surface area and porosity analyser at 77 K. Before the measurement, samples were degassed at 453 K for 6 h under vacuum. The total pore volume was calculated based on the adsorbed volume at the maximum relative pressure (P/P_0) of 0.99. The pore size of samples was calculated through Barrett-Joyner-Halenda (BJH) method from the adsorption branches of the isotherms. The Brunauer-Emmett-Teller (BET) method was used to calculate the specific surface areas. Zeta potential measurement was tested using a Zetasizer Nano-ZS from Malvern Instruments at 25 °C.

mRNA loading and release profile

5 µg of PEI-MSNs was dispersed in 10 µL of 10 mM PBS solution and mixed with 1 µL of mRNA solution (1 µg/µL) at 4 °C for 30 min (weight ratio of PEI-MSNs to mRNA=5:1). Then the mixture was centrifuged at 15,000 rpm for 10 min. 2 µL of the collected supernatant was analyzed by 'Nucleic Acid' application module at wavelength of 260 nm in a Nanodrop 1000 spectrophotometer (Thermo Scientific) to determine the amount of mRNA, using PBS as the blank. The release study was conducted by dispersing mRNA loaded nanoparticles in PBS solution at 37 °C shaking at 50 rpm for 48 h. The release

mRNA was determined by analysing the collected supernatant at selected time points using the Nanodrop.

Gel electrophoresis assay

0.5 µg of mRNA was mixed with various amounts of PEI modified MSNs (0, 5, 10, 20, 30, 40 µg) in 8 µL of 10 mM PBS. After incubation at 4 °C for 30 min, 2 µL of nucleic acid sample loading buffer (5×) was added into the mixture for a final volume of 10 µL. Then the solution was transferred into each well of the agarose gel (1%, SYBR-Safe gel stain). The electrophoresis was carried out at 80 V for 50 min, then the bands were visualized using a UV trans-illuminator (Bio-Rad).

Cellular uptake assay

The cellular uptake efficiency of PEI modified MSNs was studied in HEK293T (human embryonic kidney) cells by the inductively coupled plasma-optical emission spectrometer (ICP-OES) instrument (Vista-PRO; Varian Inc., Australia). For instance, HEK cells were seeded in a 6 well culture plate with a density of 1.25×10^5 cells per well for 24 h of incubation. Then 20 µL of PEI modified nanoparticle solution (5 mg/ml) was added to each well and incubated for another 4 h. Afterwards, the medium was removed and the cells were washed with PBS and harvested with trypsin. After another wash with PBS, cell number was counted and recorded. After centrifugation, 120 µL of DI water was added to each tube to dissolve cells under sonication for 2 h. The cells were centrifuged at 15,000 rpm for 3 min and the precipitates were dried in a 50 °C oven overnight. Finally, the silica particles were dissolved by 150 µL of NaOH solution (1 M) at room temperature for 24 h before ICP quantification.

In vitro mRNA transfection

The delivery efficacy of EGFP mRNA by PEI modified MSNs was evaluated in HEK-293T cells. The HEK-293T cells were seeded on a 12 well plate with a density of 1.2×10^5 cells/well and cultured for 24 h before transfection. 1 µg of mRNA was mixed with 40 µg of PEI modified MSNs in PBS with a total volume of 50 µL for 30 min, then mRNA-nanoparticles (NPs) formulations were added by droplets inside each well for further incubation of 48 h. The cells were collected to determine the intracellular green fluorescent protein expression by flow cytometry.

Results and discussion

TEM images of the samples synthesized at RT (MSNs-RT-*R*) are shown in Figure 1A-D. For MSNs prepared at *R*=0, 0.1, 0.2 and 0.3, the average particle size (by measuring 100 particles from TEM images) was 32, 33, 43 and 104 nm, respectively (Figure 1A-D). The pore size of MSNs was enlarged from small mesopore to large opening pore with increased *R* from 0 to 0.3, which is consistent with our previous observation.¹⁹ The typical dendritic structure was observed in MSNs-RT-0.1 (Figure 1B), which has the smallest particle size compared with DMSNs in previous reports.^{11, 13-19}

To show the difference in structures of MSNs caused by reaction temperature, MSNs-80-*R* (*R*=0, 0.1, 0.2 and 0.3) were

also prepared by increasing the reaction temperature to 80 °C while keeping the other reaction conditions unchanged. At the elevated temperature of 80 °C, the particle sizes of MSNs-80-R

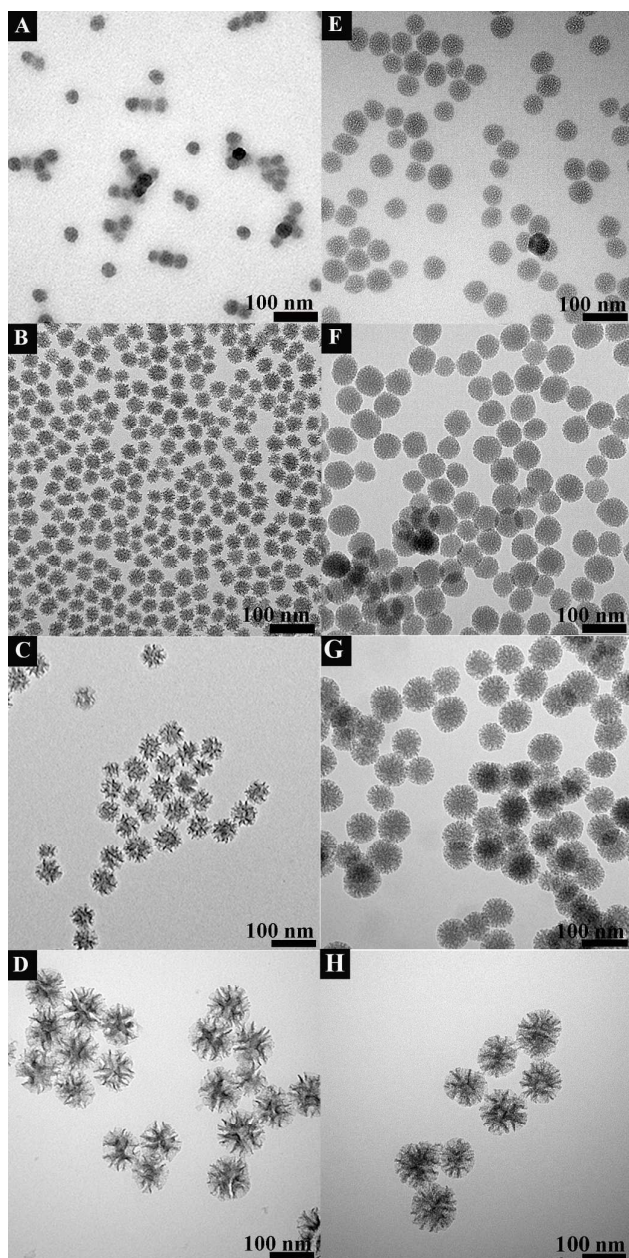
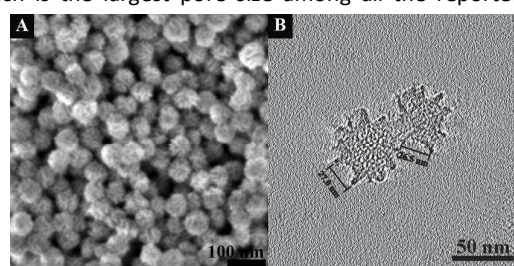


Figure 1. TEM images of MSNs-RT-0 (A), MSNs-RT-0.1 (B), MSNs-RT-0.2 (C), MSNs-RT-0.3 (D), MSNs-80-0 (E), MSNs-80-0.1 (F), MSNs-80-0.2 (G) and MSNs-80-0.3 (H)

were enlarged from 44 to 102 nm with increased R (Figure 1E-H). It is noted that at R of 0.1, only small mesopores are observed in the TEM image of MSNs-80-0.1 (Figure 1F). The dendritic pores were formed in MSNs-80-0.2 (Figure 1G) when R was increased to 0.2. It is concluded that a smaller ratio of FC4/CTAB is needed to induce the growth of dendritic structures at room temperature than at 80 °C.

The nitrogen sorption analysis was conducted to characterize the pore structures of synthesized particles. The adsorption and desorption isotherms (Figure S1A, C, E, G) of MSNs-RT- R and MSNs-80- R ($R=0, 0.1, 0.2$ and 0.3 , respectively) all exhibit type IV isotherms. Their corresponding Barrett-Joyner-Halenda (BJH) pore size distribution curves of MSNs-RT- R and MSNs-80- R samples calculated from the adsorption branches are shown in Figure S1B, D, F, H. Without FC4 ($R = 0$), MSNs-RT-0 has a small pore size of 1.1 nm (Figure S1B). Compared with MSNs-RT-0, the pore size of MSNs-80-0 is larger (2.0 nm) prepared at elevated temperature, which is explained by the increased hydrophobic volume in micelles at higher temperature.²⁰ When FC4 was used at R of 0.1, MSNs-RT-0.1 exhibited a shoulder peak centred at 5.9 nm in addition to the peak at 1.2 nm, suggesting the existence of large pores due to the penetration effect of FC4 in micelles,^{19, 21} which is consistent with the observation from TEM image (Figure 1B). The pore size of MSNs-80-0.1 is enlarged to 2.5 nm at 80 °C, suggesting the formation of slightly swollen micelles as templates for the synthesis of MSNs.¹³ With more FC4 ($R=0.2$) applied in the synthesis, the pore size of MSNs-RT-0.2 was increased to 31.7 nm while maintaining the small mesopore of 1.2 nm (Fig. S1E, F), similar to our previous study.^{13, 15-16, 19} However, MSNs-80-0.2 displayed a shoulder peak centred at 6.8 nm in addition to the peak at 2.5 nm, which is supported by TEM observation in Figure 1G. When R was further increased to 0.3, the pore sizes of both MSNs-RT-0.3 (1.4 and 31.9 nm) and MSNs-80-0.3 (2.5 and 22.3 nm) were further increased. The physical properties of MSNs are summarized in Table S1. The total pore volume increased with increased pore size while the surface area decreased as a result of enlarged particle size.²²

The above TEM images and nitrogen sorption results indicate that the room temperature synthesis favours the formation of DMSNs with larger dendritic pore and a smaller diameter than elevated temperature, and the occurrence of dendritic large pores can be induced at a lower R values. Compared to elevated temperature with the same R (FC4/CTAB), the decreased particle size at RT is explained by the slow nucleation rate⁸ and reduced micellar sizes as evidenced by the smaller pore sizes (1.1 vs 2.0 nm for MSNs-RT-0 and MSNs-80-0, respectively). Besides, at elevated temperatures such as 80 °C, the electrostatic interaction between cationic CTA⁺ and anionic FC4⁻ is weakened compared to RT,²³ leading to retarded micelle penetration and structural transformation from conventional small-pore MSNs to large-pore DMSNs.^{13, 19} Therefore, there are two advantages of room temperature synthesis: one is the formation of small particle size as the core, the other is the easy formation of dendritic large-pores on the surface of preformed core particles. Consequently, MSNs-RT-0.2 have both small sizes (diameter of 43 nm) and dendritic large-pores (26.8 nm) on the surface (Figure 1C), which is the largest pore size among all the reported MSNs



with the particle size of 50 nm.

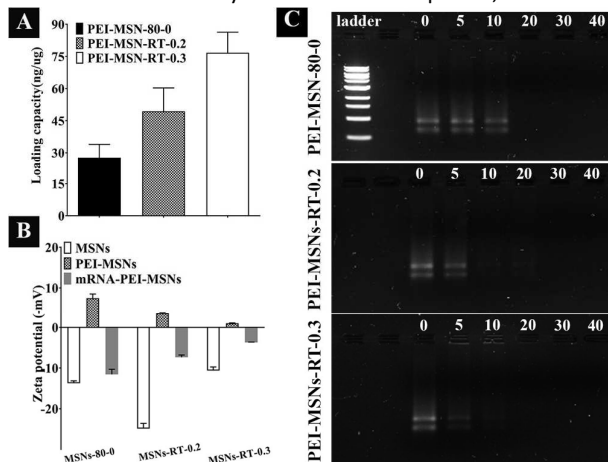
Figure 2. SEM image (A) and ET slice (B) of MSNs-RT-0.2.

To explore the detailed structure of MSNs-RT-0.2, SEM and electron tomography (ET) was further conducted to characterize MSNs-RT-0.2. The large pores can be directly observed from SEM image (Figure 2A). One ET slice (Figure 2B) revealed a core-shell structure, in which the core particle has small mesopores (< 2 nm) the shell has open and large pores (> 20 nm), supporting the mechanism we proposed before. To highlight the large pore size (~26.8 nm) and small particle size (~43 nm) of MSNs-RT-0.2, we compare this sample to MSNs-RT-0.3 with a similar pore size (22.3 nm) but a larger particle size (102 nm), as well as MSNs-80-0 with a similar particle size (44 nm) but smaller mesopore size (2.0 nm), in EGFP mRNA delivery applications. mRNA is a more effective and safer genetic molecule with sustainable expression of proteins and no risk of insertional transfection compared with DNA.²⁴⁻²⁵ Nonetheless, the intrinsic properties of mRNA include the negative surface charge repulsing the anionic cell membrane, susceptible structure as well as endosomal entrapment, are major concerns for practical applications.²⁵ A variety of nanoparticles including lipids, polymers and hybrids materials have been applied as mRNA delivery systems.²⁶⁻²⁸ However, to date, the cellular delivery of exogenous mRNA using MSNs is rarely reported.

To improve the mRNA binding and promote endosome escape, we functionalized MSNs with PEI (donated as PEI-MSNs).²⁹ The structures of MSNs were maintained as evidenced from TEM images of PEI-MSNs (Figure S2). The comparable nitrogen contents of these three MSNs were quantified to be around 5% by elemental analysis (EA, see Table S2), indicating the successful PEI modification and similar PEI content. The PEI release from MSNs was conducted at 37 °C in PBS buffer (pH 7.4). After 48 h incubation, samples were collected by centrifugation and the nitrogen contents evaluated by EA (Table S2) indicated a faster PEI molecule release from large pore sized MSNs-RT-0.2 and MSNs-RT-0.3 compared to MSNs-80-0 with the smallest pore size.

The loading capacity analysed by Nanodrop was shown in Figure 3A. PEI-MSNs-RT-0.3 possessed the highest loading capacity of 76.7 ng/μg and the loading capacity of PEI-MSNs-RT-0.2 and PEI-MSNs-80-0 were measured to be 49.4 ng/μg and 27.7 ng/μg, respectively. The highest loading capacity PEI-MSNs-RT-0.3 could be attributed to its large dendritic pores. The surface charge of three groups of MSNs and PEI-MSNs before and after mRNA loading was measured (Figure 3B). Typically, bare MSNs exhibited negative charge while the surface charge shifted to be positive after PEI modification, suggesting the successful modification of PEI on MSNs surface. Compared with mRNA-PEI-MSNs-RT-0.2 and mRNA-PEI-MSNs-RT-0.3, mRNA-PEI-MSNs-80-0 showed a negative charge of -11.6 mV because of the surface adsorption of mRNA on PEI-MSNs-80-0, which explained the lowest loading capacity compared with large pore sized DMSNs. On the other hand, the mRNA-PEI-MSNs-RT-0.3 group exhibited the lowest negative charge, implying that most of mRNA molecules were entrapped inside the mesopore rather than exposed on the outer surface.³⁰

The mRNA release study was conducted at pH 7.4, 37 °C based

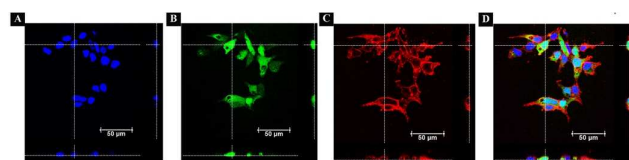


on a protocol established from a previous report.³¹ The release profile was shown in Figure S3. Among three samples, a most sustained release was observed for PEI-MSNs-80-0 during the first 24 h, with a total mRNA release of 62% at 48 h. This is explained by the least PEI released (5.5%) from PEI-MSNs-80-0 with the smallest mesopores in 48 h (Table S2). For PEI-MSNs-RT-0.2, the mRNA release rate was fast within the first 10 h, around 100% of mRNA was released at 48 h. For PEI-MSNs-RT-0.3, the released mRNA percentage was only 9% within the first 6 h, followed by a burst release in the next 4 h and 80% release of mRNA till 48 h. The PEI released from PEI-MSNs-RT-0.2 and PEI-MSNs-RT-0.3 was 11.6% and 38.9%, respectively. It is suggested that positively charged PEI conjugated with the negatively charged phosphonate surface of MSNs could be easily released from the large dendritic mesopores, but not from small mesopores. Consequently, PEI-MSNs-RT-0.2 exhibited the fastest mRNA release behaviour. The sustained release of PEI-MSNs-RT-0.3 in the first 6 h should be mainly attributed to the mRNA embedding inside the deep and dendritic large pores. With a large quantity of PEI released, a fast release behaviour similar to that of PEI-MSNs-RT-0.2 was observed afterwards.

Figure 3. EGFP mRNA loading capacity of PEI-MSNs (A). Zeta potential of MSNs, PEI-MSNs before and after EGFP mRNA loading (B). Agarose gel electrophoresis (C) of EGFP mRNA-PEI-MSNs complexes: PEI-MSNs-80-0 (upper), PEI-MSNs-RT-0.2 (middle) and PEI-MSNs-RT-0.3 (lower).

The gel retardation assay was conducted to reveal the binding affinity. The amounts of PEI-MSNs were tuned from 0 to 40 μg while the amount of mRNA was kept at a constant (0.5 μg). The mRNA only group (Figure 3C) showed the complete electrophoretic shift. For the PEI-MSNs treated group, the band intensity of shifted mRNA decreased with the increased amount of NPs. When 5 μg of NPs were applied, compared with small sized PEI-MSNs-80-0, both PEI-MSNs-RT-0.2 and PEI-MSNs-RT-0.3 with dendritic pore channels possessed weaker intensity of shifted mRNA, supporting the stronger interaction between mRNA molecules and rough DMSNs with unique opening pore, consistent with our previous report in plasmid binding.³⁰ The relatively weak band intensity of PEI-MSNs-RT-0.3 suggested the stronger binding affinity than PEI-MSNs-RT-0.2 contributed by the deep dendritic pore channel to separate and embed mRNA in the mesopore. No shifted mRNA was observed for PEI-MSNs-RT-0.2 and PEI-MSNs-RT-0.3

when the amount of NPs was increased to 10 μg , indicating the complete binding between mRNA and PEI-DMSNs, while the released mRNA was still observed for PEI-MSNs-80-0. When the amount of NPs was further increased to 20 or more, the



mRNA was completely

Figure 4. Orthogonal side-views from z-stack confocal images confirm the successful cellular uptake of PEI-MSNs-RT-0.2. Fluorescent images (A) from the blue channel, showing nucleus stained with DAPI; (B) from the green channel, showing PEI-MSNs-RT-0.2 labelled with FITC; (C) from the red channel, showing cell membrane stained with DIL and (D) overlaid images of (A-C). Pictures of the XY plane and the side views along the dashed lines are presented in (D). Scale bar: 50 μm .

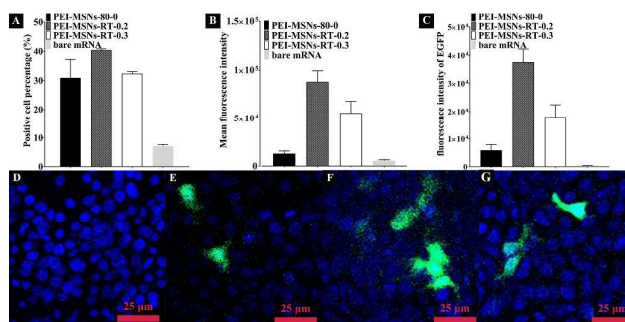
retained in the well for all the NPs. The above results revealed the strong interaction between mRNA molecules and DMSNs due to the nanotopography.

The intracellular delivery of EGFP mRNA was conducted by incubation of human embryonic kidney cells 293 (HEK293T) normal cells with mRNA-PEI-MSNs for 48 h. The cellular uptake of PEI-MSNs was quantified by determining the silicon content in each cell measured by ICP-OES.³² The silicon amount per cell (Table S3) indicated the similar cellular uptake of PEI-MSNs-80-0 and PEI-MSNs-RT-0.2 with similar particle sizes. In contrast, PEI-MSNs-RT-0.3 possessing a relative larger particle size showed lower silicon content in cells, suggesting smaller-sized particles contributed to a higher cellular uptake.⁴ The successful cellular uptake was also demonstrated using three dimensional Z-stack confocal microscopy analysis (Figure 4). The overlapping of green fluorescence (from FITC labelled nanoparticles) and blue fluorescence (from DAPI labelled nucleus) was within the red color (from DIL stained cell membrane) from side view in Fig 4D, suggesting that the co-localization of nanoparticles and nucleus inside the cells and the nanoparticles were uptaken by cells.

The cell viability of HEK293T cells treated with PEI-MSNs was evaluated using 3-(4,5-dimethylthiazol-2-yl)-2,5-diphenyltetrazolium bromide (MTT) assay. As shown in Figure S4, all PEI-MSNs exhibited dose dependent cytotoxicity and retained good biocompatibility, showing >80% viability at dosages ranging from 10 to 40 $\mu\text{g}/\text{ml}$.

The expressed EGFP level was quantified by fluorescence activated cell sorting (FACS) analysis. As shown in Figure 5A, mRNA alone showed limited GFP expression. mRNA-PEI-MSNs-RT-0.2 complexes showed the highest mean fluorescence intensity (MFI) due to the strong binding affinity and high cellular uptake contributed by the dendritic nanotopography and small diameter respectively. In comparison, the low MFI of PEI-MSNs-80-0 was attributed to weak binding affinity limited by the small mesopore while the large particle size of PEI-MSNs-RT-0.3 limited the cellular uptake and efficient intracellular expression of EGFP. The transfection efficacy (Figure 5B) of mRNA-PEI-MSNs-RT-0.2 was 40.4%, higher than both mRNA-PEI-MSNs-80-0 and mRNA-PEI-MSNs-RT-0.3 complexes because of the small diameter. The fluorescence intensity of EGFP was further calculated by multiplying MFI

with positive cell percentage. To be noted, the mRNA-PEI-MSNs-RT-0.2 complex (Figure 5C) exhibited much higher fluorescence intensity of EGFP compared with other two. Lipofectamine was also included as the positive control, which showed a higher transfection efficacy (81%) compared to PEI-



MSNs-RT-0.2,

Figure 5. EGFP expression levels in HEK293T cells determined by flow cytometry after treatment with mRNA and PEI-MSNs groups: Mean fluorescence intensity (A), Positive cell percentage (B) and fluorescence intensity per positive cell (C) and confocal microscopy images of EGFP expression in HEK293T cells treated with PBS (D), mRNA-PEI-MSNs-80-0 (E), mRNA-PEI-MSNs-RT-0.2 (F) and mRNA-PEI-MSNs-RT-0.3 (G).

suggesting that there is still plenty of room to further improve the transfection efficiency of silica-based nano-vectors.

The EGFP mRNA expression was also analyzed by confocal microscopy (Figure 5D-G). The images were taken for HEK-293T cells incubated with different PEI-MSNs and mRNA complexes for 48 h using PBS treated cells as the control group (Figure 4D). PEI-MSNs-RT-0.2 group (Figure 5F) exhibited higher green fluorescence intensity (indicating EGFP expression level) than PEI-MSNs-80-0 (Figure 5E) and PEI-MSNs-RT-0.3 (Figure 5G) groups. The observation from confocal microscopy images was consistent with the quantitative results from flow cytometry (Figure 5A-C). The transfection result indicates that the small sized DMSNs with large pore size favour efficient mRNA transfection *in vitro*.

Conclusions

DMSNs with small diameter and large pore size have been prepared at room temperature for the first time and applied for mRNA delivery as a proof of concept. The rational choice of room temperature is the key towards the successful synthesis of small particle size and dendritic large pores. This new finding is important for developing a delivery platform with small particle size for efficient cellular uptake and large pore size for biomacromolecules in a range of bio-applications.

Conflicts of Interest

The authors declare no competing financial interest

Acknowledgement

We thank the support from Australian Research Council, the Australian Microscopy & Microanalysis Research Facility at the Centre for Microscopy and Microanalysis, the University of Queensland, and the Queensland node of the Australian National Fabrication Facility (ANFF).

References

- Du, X.; Shi, B. Y.; Liang, J.; Bi, J. X.; Dai, S.; Qiao, S. Z., Developing Functionalized Dendrimer-Like Silica Nanoparticles with Hierarchical Pores as Advanced Delivery Nanocarriers. *Adv Mater* **2013**, *25* (41), 5981-5985.
- Tang, F. Q.; Li, L. L.; Chen, D., Mesoporous Silica Nanoparticles: Synthesis, Biocompatibility and Drug Delivery. *Adv Mater* **2012**, *24* (12), 1504-1534.
- Bouchoucha, M.; Cote, M. F.; C-Gaudreault, R.; Fortin, M. A.; Kleitz, F., Size-Controlled Functionalized Mesoporous Silica Nanoparticles for Tunable Drug Release and Enhanced Anti-Tumoral Activity. *Chem Mater* **2016**, *28* (12), 4243-4258.
- Lu, F.; Wu, S. H.; Hung, Y.; Mou, C. Y., Size Effect on Cell Uptake in Well-Suspended, Uniform Mesoporous Silica Nanoparticles. *Small* **2009**, *5* (12), 1408-1413.
- Pan, L. M.; He, Q. J.; Liu, J. N.; Chen, Y.; Ma, M.; Zhang, L. L.; Shi, J. L., Nuclear-Targeted Drug Delivery of TAT Peptide-Conjugated Monodisperse Mesoporous Silica Nanoparticles. *J Am Chem Soc* **2012**, *134* (13), 5722-5725.
- Kim, M. H.; Na, H. K.; Kim, Y. K.; Ryoo, S. R.; Cho, H. S.; Lee, K. E.; Jeon, H.; Ryoo, R.; Min, D. H., Facile Synthesis of Monodispersed Mesoporous Silica Nanoparticles with Ultralarge Pores and Their Application in Gene Delivery. *ACS Nano* **2011**, *5* (5), 3568-3576.
- Gan, Q.; Dai, D. W.; Yuan, Y.; Qian, J. C.; Sha, S.; Shi, J. L.; Liu, C. S., Effect of size on the cellular endocytosis and controlled release of mesoporous silica nanoparticles for intracellular delivery. *Biomed Microdevices* **2012**, *14* (2), 259-270.
- Yu, M. H.; Zhou, L.; Zhang, J.; Yuan, P.; Thorn, P.; Gu, W. Y.; Yu, C. Z., A simple approach to prepare monodisperse mesoporous silica nanospheres with adjustable sizes. *J Colloid Interf Sci* **2012**, *376*, 67-75.
- Na, H. K.; Kim, M. H.; Park, K.; Ryoo, S. R.; Lee, K. E.; Jeon, H.; Ryoo, R.; Hyeon, C.; Min, D. H., Efficient Functional Delivery of siRNA using Mesoporous Silica Nanoparticles with Ultralarge Pores. *Small* **2012**, *8* (11), 1752-1761.
- Du, X.; Qiao, S. Z., Dendritic Silica Particles with Center-Radial Pore Channels: Promising Platforms for Catalysis and Biomedical Applications. *Small* **2015**, *11* (4), 392-413.
- Polshettiwar, V.; Cha, D.; Zhang, X. X.; Basset, J. M., High-Surface-Area Silica Nanospheres (KCC-1) with a Fibrous Morphology. *Angew Chem Int Edit* **2010**, *49* (50), 9652-9656.
- Abbaraju, P. L.; Yang, Y.; Yu, M.; Fu, J.; Xu, C.; Yu, C., Core-Shell-structured Dendritic Mesoporous Silica Nanoparticles for Combined Photodynamic Therapy and Antibody Delivery. *Chem Asian J* **2017**, *12* (13), 1465-1469.
- Xu, C.; Yu, M. H.; Noonan, O.; Zhang, J.; Song, H.; Zhang, H. W.; Lei, C.; Niu, Y. T.; Huang, X. D.; Yang, Y. N.; Yu, C. Z., Core-Cone Structured Monodispersed Mesoporous Silica Nanoparticles with Ultra-large Cavity for Protein Delivery. *Small* **2015**, *11* (44), 5949-5955.
- Yang, Y. N.; Bernardi, S.; Song, H.; Zhang, J.; Yu, M. H.; Reid, J. C.; Strounina, E.; Searles, D. J.; Yu, C. Z., Anion Assisted Synthesis of Large Pore Hollow Dendritic Mesoporous Organosilica Nanoparticles: Understanding the Composition Gradient. *Chem Mater* **2016**, *28* (3), 704-707.
- Yu, Y. J.; Xing, J. L.; Pang, J. L.; Jiang, S. H.; Lam, K. F.; Yang, T. Q.; Xue, Q. S.; Zhang, K.; Wu, P., Facile Synthesis of Size Controllable Dendritic Mesoporous Silica Nanoparticles. *ACS Appl Mater Inter* **2014**, *6* (24), 22655-22665.
- Zhang, K.; Xu, L. L.; Jiang, J. G.; Calin, N.; Lam, K. F.; Zhang, S. J.; Wu, H. H.; Wu, G. D.; Albel, B.; Bonneviot, L.; Wu, P., Facile Large-Scale Synthesis of Monodisperse Mesoporous Silica Nanospheres with Tunable Pore Structure. *J Am Chem Soc* **2013**, *135* (7), 2427-2430.
- Moon, D. S.; Lee, J. K., Tunable Synthesis of Hierarchical Mesoporous Silica Nanoparticles with Radial Wrinkle Structure. *Langmuir* **2012**, *28* (33), 12341-12347.
- Shen, D. K.; Yang, J. P.; Li, X. M.; Zhou, L.; Zhang, R. Y.; Li, W.; Chen, L.; Wang, R.; Zhang, F.; Zhao, D. Y., Biphasic Stratification Approach to Three-Dimensional Dendritic Biodegradable Mesoporous Silica Nanospheres. *Nano Lett* **2014**, *14* (2), 923-932.
- Wang, Y.; Nor, Y. A.; Song, H.; Yang, Y. N.; Xu, C.; Yu, M. H.; Yu, C. Z., Small-sized and large-pore dendritic mesoporous silica nanoparticles enhance antimicrobial enzyme delivery. *J Mater Chem B* **2016**, *4* (15), 2646-2653.
- Kruk, M.; Jaroniec, M.; Sayari, A., A unified interpretation of high-temperature pore size expansion processes in MCM-41 mesoporous silicas. *J Phys Chem B* **1999**, *103* (22), 4590-4598.
- Yang, S.; Zhou, X. F.; Yuan, P.; Yu, M. H.; Xie, S. G.; Zou, J.; Lu, G. Q.; Yu, C. Z., Siliceous nanopods from a compromised dual-templating approach. *Angew Chem Int Edit* **2007**, *46* (45), 8579-8582.
- Dai, F.; Zai, J. T.; Yi, R.; Gordin, M. L.; Sohn, H.; Chen, S. R.; Wang, D. H., Bottom-up synthesis of high surface area mesoporous crystalline silicon and evaluation of its hydrogen evolution performance. *Nat Commun* **2014**, *5*.
- Zhang, L. M.; Kang, W. L.; Xu, D. R.; Feng, H. S.; Zhang, P. Y.; Li, Z.; Lu, Y.; Wu, H. R., The rheological characteristics for the mixtures of cationic surfactant and anionic-nonionic surfactants: the role of ethylene oxide moieties. *Rsc Adv* **2017**, *7* (22), 13032-13040.
- Curtin, C. M.; Tierney, E. G.; McSorley, K.; Cryan, S. A.; Duffy, G. P.; O'Brien, F. J., Combinatorial Gene Therapy Accelerates Bone Regeneration: Non-Viral Dual Delivery of VEGF and BMP2 in a Collagen-Nanohydroxyapatite Scaffold. *Adv Healthc Mater* **2015**, *4* (2), 223-227.
- Islam, M. A.; Reesor, E. K. G.; Xu, Y. J.; Zope, H. R.; Zetter, B. R.; Shi, J. J., Biomaterials for mRNA delivery. *Biomater Sci-Uk* **2015**, *3* (12), 1519-1533.
- Oberli, M. A.; Reichmuth, A. M.; Dorkin, J. R.; Mitchell, M. J.; Fenton, O. S.; Jaklenc, A.; Anderson, D. G.; Langer, R.; Blankschtein, D., Lipid Nanoparticle Assisted mRNA Delivery for Potent Cancer Immunotherapy. *Nano Lett* **2017**, *17* (3), 1326-1335.
- Guan, S.; Rosenecker, J., Nanotechnologies in delivery of mRNA therapeutics using nonviral vector-based delivery systems. *Gene Ther* **2017**, *24* (3), 133-143.
- Persano, S.; Guevara, M. L.; Li, Z. Q.; Mai, J. H.; Ferrari, M.; Pompa, P. P.; Shen, H. F., Lipopolyplex potentiates anti-tumor immunity of mRNA-based vaccination. *Biomaterials* **2017**, *125*, 81-89.
- Xia, T. A.; Kovochich, M.; Liong, M.; Meng, H.; Kabehie, S.; George, S.; Zink, J. I.; Nel, A. E., Polyethyleneimine Coating Enhances the Cellular Uptake of Mesoporous Silica Nanoparticles and Allows Safe Delivery of siRNA and DNA Constructs. *ACS Nano* **2009**, *3* (10), 3273-3286.

Journal Name

LETTER

30. Song, H.; Yu, M.; Lu, Y.; Gu, Z.; Yang, Y.; Zhang, M.; Fu, J.; Yu, C., Plasmid DNA Delivery: Nanotopography Matters. *J Am Chem Soc* **2017**, *139* (50), 18247-18254.
31. Palama, I. E.; Cortese, B.; D'Amone, S.; Gigli, G., mRNA delivery using non-viral PCL nanoparticles. *Biomater Sci-Uk* **2015**, *3* (1), 144-151.
32. Chou, L. Y. T.; Zagorovsky, K.; Chan, W. C. W., DNA assembly of nanoparticle superstructures for controlled biological delivery and elimination. *Nat Nanotechnol* **2014**, *9* (2), 148-155.